Scientific
Research
Publishing

Dynamic Analysis of an Algae-Fish Harvested Model with Allee Effect

Xiaoyu Song[1,2], Hengguo Yu[1,2*], Min Zhao[2,3*]

[1]School of Mathematics and Physics, Wenzhou University, Wenzhou, China
[2]Key Laboratory for Subtropical Oceans & Lakes Environment and Biological Resources Utilization Technology of Zhejiang, Wenzhou University, Wenzhou, China
[3]School of Life and Environmental Science, Wenzhou University, Wenzhou, China
Email: *yuhengguo5340@163.com, *zhaomin-zmcn@tom.com

Abstract

In this paper, an algae-fish harvested model with Allee effect was established to further explore the dynamic evolution mechanism under the influence of key factors. Mathematical theoretical work not only investigated the existence and stability of all possible equilibrium points, but also probed into the occurrence of transcritical and Hopf bifurcation. The numerical simulation works verified the effectiveness of the theoretical derivation results and displayed rich bifurcation dynamical behaviors, which showed that Allee effect and harvest have played a vital role in the dynamic relationship between algae and fish. In summary, it was expected that these research results would be beneficial for promoting the study of bifurcation dynamics in aquatic ecosystems.

Keywords

Algae and Fish Model, Allee Effect, Harvesting, Equilibrium Point, Bifurcation

1. Introduction

Water is the source of life, but with the rapid development of economy, eutrophication of lakes and reservoirs has become one of the universal environmental problems in the world. One of the most abhorrent performance characteristics of eutrophication in lakes and reservoirs is the appearance of cyanobacterial blooms [1]. When cyanobacterial blooms appear in lakes and reservoirs, the water surface is covered by a thick layer of bloom, and the cyanobacterial population constituting the bloom, breed in large quantities and then die in large

quantities. The dead cyanobacteria emit an unbearable fishy odor during the decomposition process, and at the same time consume a lot of dissolved oxygen in the water, causing a large number of fish, shrimp and other aquatic animals to die of suffocation. Cyanobacterial blooms also tend to block the water filtration facilities of the waterworks, leading to water supply failures, and greatly increase the amount of disinfectant. More seriously, the bloom contains a class of toxins called microcystins, which is considered to be a strong cancer-promoting substance. State Environmental Protection Administration released information shows that nearly 1/4 of China's rivers due to pollution cannot meet the water quality requirements of agricultural irrigation water standards, the degree of algae pollution of the China's natural water bodies deepen year by year, such as large-scale outbreaks of cyanobacterial blooms in Tai Lake, Chaohu Lake and Dianchi Lake, which are vividly called "ecological cancer" [2]. It seriously affects people's production and life. Therefore, the way to reduce the eutrophication of water bodies is one of the research hotspots that many scholars are very concerned about.

The purification technology of eutrophication water body mainly includes physical, chemical and biological method. Compared with the other two methods, biological method not only produces less pollution, but also is cheap and easy to operate [3] [4] [5]. Among which there are two most economical, effective and reasonable ways: one is to grow aquatic plants. However, its disadvantages are large investment, high labor intensity, low economic value, and aquatic plants are only suitable for planting and growing in shallow water areas, which must be cleaned regularly, otherwise it is easy to cause secondary pollution. The other is to put filter-feeding fish. Silver carp and bighead carp are unique to China's ecological water purification fish, which has been introduced to 27 countries for biological purification of eutrophic water bodies, and have received good results. In the field of aquatic ecology, Shapiro *et al.* (1975) were the first to propose the classical biological manipulation theory [6] [7], the main principle of which is to adjust the structure of fish populations, protect and develop phytophagous zooplankton, so as to control the overgrowth of algae, and the core of which is the use of zooplankton to filter feeding on planktonic algae and increase the transparency of the water body [8] [9]. Studies guided by classical biological manipulation theory have shown that increasing zooplankton populations can effectively reduce phytoplankton populations, increase the transparency of water body, and achieve the purpose of improving water quality [7]. However, with the emergence of a large number of large carnivorous zooplanktons, small zooplanktons that feed on phytoplankton in the water body, such as rotifers and small cladoceras, are subjected to high-intensity attacks and their numbers decrease significantly, which reduces predation pressure on phytoplankton and results in an inverse elastic mass growth of phytoplankton [10]. Therefore, the opposite pathway to classical biological manipulation, the non-classical biological control theory of directly controlling phytoplankton populations by stocking filter-feeding fish, is now widely used.

The non-classical biological manipulation theory was put forward by Chinese scholars Liu Jiankang and Xie Ping [11], and the main method is to put phytoplankton-eating fish to control algae directly or to reduce the number of aggressive fish to control algae indirectly. Numerous studies have shown that releasing silver carp and bighead carp directly to the water surface successfully controlled cyanobacterial blooms, reduced phytoplankton and zooplankton biomass, total phosphorus (TP), total nitrogen (TN), and COD to varying degrees, and also mitigated the degree of eutrophication in the water body and effectively improved water quality [12] [13] [14] [15]. Lake Kasumigaura in Japan in the 1970s, by industrial production, overfishing and other factors, the water quality has been extensively polluted. In the summer of 1973, the dissolved oxygen in the algal bloom area was greatly reduced, resulting in a large number of carp deaths and serious eutrophication. After that, the Chinese mixed culture model was adopted to release silver carp and bighead carp, and the water quality has been greatly improved, and the clear lake has once again become a beautiful tourist destination. In the research of cyanobacteria bloom control technology in the lake, relevant experts of the Institute of Hydrology have explored and innovated, and summarized the biological manipulation method of using filter-feeding fish to directly control cyanobacteria blooms, and also uncovered the mystery of the disappearance of cyanobacteria bloom in the East Lake of Wuhan for 15 consecutive years. The protection and treatment of Dianchi Lake revolve around the six major projects of lake pollution interdiction, ecological restoration, river management, sediment dredging, water source protection, and water diversion in the outer basin. In recent years, a large number of silver carp and bighead carp have been released to control algae, and certain results have been achieved [1].

Silver carp and bighead carp are used to control algae because of their special feeding organs. Silver carp have spongy gill rakers, and bighead carp have comb-like gill rakers, which are able to filter algae effectively. Furthermore, silver carp and bighead carp have long intestinal tract with good digestibility of phytoplankton. After filter feeding on algae, the water quality changed from turbidity to freshness [16]. Silver carp and bighead carp are medium-sized fish, which have the characteristics of fast growth and easy catching. Therefore, silver carp and bighead carp become the main biological tools for algal control through atypical biological manipulation. The daily filter feeding of silver carp and bighead carp could reach 12.5 percent and 9.5 percent of their body weight respectively. Silver carp and bighead carp are natural free-range green foods with high protein and low fat. For every kilogram of fish weight gain, 32 grams of nitrogen and 4.5 grams of phosphorus in the water are converted into high-quality protein. Catching a certain amount of fish from the water body is equivalent to transferring a large amount of nitrogen, phosphorus and other nutrient elements out of the water body, which can greatly reduce the degree of eutrophication of the water body. Ecological fishery is one of the most effective means to purify water quality of reservoir and maintain ecological balance. Therefore, it is very important to make a reasonable plan for releasing and catching of filter-feeding

fish in reservoirs and lakes, and dynamically adjust the stocking ratio of silver carp and bighead carp [2], so as to achieve the optimal proportion of plankton in the water body of reservoirs and lakes.

2. Algae-Fish Ecological Model Formulation

The interactions between populations are important and complex in ecology. It is an effective method to study the dynamic behavior of populations by building mathematical models close to reality, and scholars have built various types of models to study interspecific interactions in biology. The establishment of the well-known Lotka-Volterra model solves the key problem of how to express population interactions in nature through mathematical models [17] [18]. Applied mathematicians usually use mathematical model as a tool to study the complex dynamic behavior between predator and prey, because the interaction between predator and prey is widespread in nature. It plays an important role in ecological research, so the study of predator-prey model will continue to play an important role in biomathematics [19] [20]. The classic predator-prey model can be represented by the following ordinary differential equation:

$$\begin{cases} \dfrac{\mathrm{d}x}{\mathrm{d}t} = r_1 x \left(1 - \dfrac{x}{k} \right) - g(x,y)y, \\ \dfrac{\mathrm{d}y}{\mathrm{d}t} = r_2 y + h(x,y)y - \beta y, \end{cases} \tag{2.1}$$

where $x(t)$ and $y(t)$ are the population densities of prey and predators, respectively. As we all know, due to the constraints of the same species competition, environmental factors and other mechanisms, the population in nature cannot grow indefinitely. Allowing a prey population to grow logically is a common modeling method in the form $r_1 x \left(1 - \dfrac{x}{k} \right)$, where r_1 is the intrinsic growth rate of the prey and k is the maximum environmental capacity. The role of the functional response term is to connect the predator and prey, that is, the prey biomass consumed by each predator per unit time, which is described by $g(x,y)$, while $h(x,y)$ is called the functional response of the predator [21], indicating the growth rate obtained by the predator through the consumption of prey. Common functional responses are generally divided into two categories. Namely, predator-dependent functional response and prey-dependent functional response.

From the perspective of human needs, the sustainable development and harvesting of biological resources is necessary [22]. Common harvest terms in dynamic systems include constant harvest terms, proportional harvest terms, and nonlinear harvest terms [23]-[28]. Chakraborty *et al.* considered a ratio-dependent predator-prey model [29], in which the predator population is harvested at unit harvest intensity. It is reasonable and realistic to select the unit of harvest intensity for harvesting [30]. Chakraborty *et al.*'s research results show that the coexistence of predators and prey, which is often observed in nature, is difficult to observe in the laboratory. One important reason is lack of higher predators, and

harvest plays the role of this higher predator, allowing predator and prey to coexist. Therefore, harvest has a great impact on the dynamic behavior of biological populations [31]. It is also more reasonable to consider harvest terms in the model.

In the population dynamics, the cluster life style of the biological population is conducive to the growth of the population, but the excessive cluster density often leads to the growth of the biological population due to resource competition. The population density is too sparse or too dense, which is not conducive to survival and development of the population. For each population, there is an independent optimal growth and reproductive density, a mechanism called the Allee effect [32] [33] [34]. Allee effect is generally divided into strong Allee effect and weak Alee effect [35] [36]. When the population has a weak Allee effect, although the population density growth is slow, the population density growth is positive. However, when a species with sparse population density is subjected to a strong Allee effect, the population will eventually become extinct. In 1931, Warder Clyde Allee showed that Allee effect exist during the growth of prey in real ecosystems. In fact, not only animals, most organisms have this characteristic, and even the initial population size of the pathogen must be large enough to continue to grow, below a certain number will no longer grow or even decline. The Allee effect occurs through a variety of mechanisms, including inbreeding decline, lack of cooperative feeding, inability to defend against predators, mating failure, and time asynchronous reproductive maturation of both sexes [34]. Alee effect terms are usually introduced into model by addition and multiplication in mathematical model [34] [37] [38] [39] [40]. The study of Allee effect has achieved rich results. Sen *et al.* discussed the effect of Alee effect in the form of $(x - \beta)$ on the population dynamics of predators in the model of one predator and two prey [41], where x is the population density and β is the diaphragm value of the Allee effect. Liu *et al.* established a host-parasite model with Allee effect and found that Allee effect can alleviate dynamic complexity [42]. The reaction-diffusion predator-prey model with Allee effect has also been extensively studied. Liu *et al.* found that weak Alee effect in the form of $\dfrac{A}{x + A}$ and time delay can control the change of pattern shape [43], where x is the population density and A is the threshold of Allee effect. Wang *et al.* found that in the reaction-diffusion predator-prey model, Allee effect can cause instability and form a cavity mode [44].

Based on the above analysis, we will construct an algae-fish harvested ecological model with Allee effect, which can be described by the following differential equations:

$$\begin{cases} \dfrac{\mathrm{d}x}{\mathrm{d}t} = r_1 x \left(1 - \dfrac{x}{k}\right)\left(\dfrac{x}{n} - 1\right) - mxy - q_1 ex, \\ \dfrac{\mathrm{d}y}{\mathrm{d}t} = r_2 y + \delta(1 - \alpha)mxy - \beta y - q_2 ey, \end{cases} \tag{2.2}$$

where all the parameters are positive and $n(0 < n < k)$ is Allee effect threshold, the prey population is doomed to extinction when the prey population density or size is below the threshold. r_2 is intrinsic growth rate of biological manipulation predator, β is the mortality rate of biological manipulation predator, δ is the energy conversion rate, α is the assimilated food of catabolic loss during the predation period, e is the harvesting effort of fish and $q_i(i=1,2)$ represents the catchability coefficients of algae and fish respectively. The biological significance of other parameters in the model (2.1) is consistent.

In order to simplify the model (2.2), we take the following transformations as

$$\mu = \delta(1-\alpha), e_1 = q_1 e, e_2 = q_2 e,$$

then the model (2.2) can be rewritten as

$$\begin{cases} \dfrac{dx}{dt} = r_1 x \left(1 - \dfrac{x}{k}\right)\left(\dfrac{x}{n} - 1\right) - mxy - e_1 x, \\ \dfrac{dy}{dt} = r_2 y + \mu mxy - \beta y - e_2 y, \end{cases} \tag{2.3}$$

according to biology meaning, we just need to explore the model (2.3) within $R_2^+ = \{(x,y) : x > 0, y \geq 0\}$.

The rest of the present paper is organized as follows. In Section 3, we give the critical conditions for the existence and stability of each equilibrium, as well as the existence of limit cycles. In Section 4, we discuss the local bifurcations of model (2.3), such as transcritical bifurcation, and Hopf bifurcation. With the help of numerical simulation, the dynamic behaviors of model (2.3) are studied when bifurcation occurs in Section 5. Finally, the paper makes a brief summary in Section 6.

3. Results of Mathematical Analysis

Equilibrium points are the special solutions, which will exhibit rich properties of the model (2.3). Therefore, the existence and stability of all possible equilibrium points of the model (2.3) will be discussed in this section, and we will also use the Poincare-Bendixson theorem to confirm the existence of a limit cycle.

3.1. Existence of Equilibrium Point

In order to obtain the equilibria of the model (2.3), we consider the prey nullcline and predator nullcline of the model, which are given by:

$$\begin{cases} F_1(x,y) = r_1 x \left(1 - \dfrac{x}{k}\right)\left(\dfrac{x}{n} - 1\right) - mxy - e_1 x = 0, \\ F_2(x,y) = r_2 y + \mu mxy - \beta y - e_2 y = 0. \end{cases} \tag{3.1}$$

It is obvious that the model (2.3) has one trivial extinction equilibrium point $E_0(0,0)$ and two predator-free equilibrium points $E_1(x_1,0)$ and $E_2(x_2,0)$. The equilibrium point E_0 exists unconditionally. Where x_1 and x_2 are the roots of the equation:

$$r_1 x^2 - r_1 (k+n) x + (r_1 + e_1) kn = 0,$$

then we can obtain the concrete expressions of x_1 and x_2 as

$$x_1 = \frac{r_1 (k+n) + \sqrt{\Delta}}{2r_1}, \quad x_2 = \frac{r_1 (k+n) - \sqrt{\Delta}}{2r_1},$$

where

$$\Delta = r_1^2 (k+n)^2 - 4r_1 kn (r_1 + e_1).$$

The analysis shows that when $e_1 = \dfrac{r_1 (k-n)^2}{4kn}$, there is only one boundary equilibrium point $\left(\dfrac{k+n}{2}, 0 \right)$, but at this time the model (2.3) does not have an internal equilibrium point, the predator population becomes extinct, and the model (2.3) does not persist. Therefore, we consider the case when there are two boundary equilibrium points, which need to satisfy $e_1 < \dfrac{r_1 (k-n)^2}{4kn}$.

For the possible positive internal equilibria, we only need consider the positive solutions of the following equations:

$$\begin{cases} y = \dfrac{r_1 \left(1 - \dfrac{x}{k}\right)\left(\dfrac{x}{n} - 1\right) - e_1}{m}, \\ r_2 + \mu m x - \beta - e_2 = 0, \end{cases}$$

then we can obtain the concrete expressions for the internal equilibrium point as

$$E_3 = (x_3, y_3) = \left(\frac{\beta + e_2 - r_2}{\mu m}, \frac{r_1 \left(1 - \dfrac{x_3}{k}\right)\left(\dfrac{x_3}{n} - 1\right) - e_1}{m} \right).$$

Considering the biological significance as well as the characteristics of isocline lines, we know that the existence of internal equilibrium point is conditional, $\dfrac{r_1 (k+n) - \sqrt{\Delta}}{2r_1} < x_3 < \dfrac{r_1 (k+n) + \sqrt{\Delta}}{2r_1}$ and $e_2 > r_2 - \beta$ must be satisfied. Therefore, we obtain the following conclusions about the existence of internal equilibrium point. If the internal equilibrium point does not exist, the model (2.3) is not persistent. Filterfeeding fish will tend to extinction, which is not conducive to ecological balance. So, it is important for us to study complex dynamic characteristics of the model (2.3). From the above analysis, we have known the existence condition of equilibrium point, and the following studies the stability of the internal equilibrium point when it exists.

3.2. Stability of Equilibrium Point

The stability of equilibrium points can be obtained through the signs of the eigenvalues of the Jacobian matrix. The Jacobian matrix of the model (2.3) at an arbitrary equilibrium point $E(x, y)$ is given by

$$J_{E(x,y)} = \begin{pmatrix} r_1\left(1-\dfrac{x}{k}\right)\left(\dfrac{x}{n}-1\right) - my - e_1 + \dfrac{-2r_1x^2 + (n+k)r_1x}{kn} & -mx \\ \mu my & r_2 + \mu mx - \beta - e_2 \end{pmatrix},$$

then we have the following theorems about the stability of equilibrium points.

Theorem 3.2.1. $E_0(0,0)$ is a stable node point when $e_2 > r_2 - \beta$, but E_0 is an unstable saddle point when $e_2 < r_2 - \beta$.

Proof:

The Jacobian matrix at the boundary equilibrium point $E_0(0,0)$ can be written as:

$$J_{E_0(0,0)} = \begin{pmatrix} -r_1 - e_1 & 0 \\ 0 & r_2 - \beta - e_2 \end{pmatrix}.$$

Obviously $J_{E_0(0,0)}$ has two eigenroots $\lambda_1 = -r_1 - e_1 < 0$, and $\lambda_2 = r_2 - \beta - e_2$. Thereby, if $e_2 > r_2 - \beta$, then $\lambda_2 < 0$, and E_0 is a stable node or focus point; if $e_2 < r_2 - \beta$, then $\lambda_2 > 0$, and E_0 is an unstable saddle point. This completes the proof.

Theorem 3.2.2. $E_1\left(\dfrac{r_1(k+n) + \sqrt{r_1^2(k+n)^2 - 4r_1kn(r_1+e_1)}}{2r_1}, 0\right)$ is a stable node

point when $e_2 > r_2 - \beta + \mu mx_1$, but E_1 is an unstable saddle point when $e_2 < r_2 - \beta + \mu mx_1$.

Proof: The expression of the Jacobian matrix around the equilibrium point E_1 is given by:

$$J_{E_1} = \begin{pmatrix} \dfrac{-2r_1x_1^2 + (n+k)r_1x_1}{kn} & -mx_1 \\ 0 & r_2 + \mu mx_1 - \beta - e_2 \end{pmatrix}.$$

The eigenvalues of J_{E_1} are

$$\lambda_1 = \dfrac{-2r_1x_1^2 + (n+k)r_1x_1}{kn} = \dfrac{\left[-r_1(k+n) - \sqrt{\Delta}\right]\sqrt{\Delta}}{2r_1kn} < 0, \quad \lambda_2 = r_2 + \mu mx_1 - \beta - e_2.$$

Thereby, if $e_2 > r_2 - \beta + \mu mx_1$, then $\lambda_2 < 0$, and E_1 is a stable node or focus point; if $e_2 < r_2 - \beta + \mu mx_1$, then $\lambda_2 > 0$, and E_1 is an unstable saddle point. This completes the proof.

Theorem 3.2.3. $E_2\left(\dfrac{r_1(k+n) - \sqrt{r_1^2(k+n)^2 - 4r_1kn(r_1+e_1)}}{2r_1}, 0\right)$ always exists

as an unstable equilibrium point. When $e_2 < r_2 - \beta + \mu mx_2$, E_2 is an unstable node or focus point, otherwise E_2 is an unstable saddle point if $e_2 > r_2 - \beta + \mu mx_2$.

Proof: The Jacobian matrix of the model (2.3) evaluated at E_2 is:

$$J_{E_2} = \begin{pmatrix} \dfrac{-2r_1x_2^2 + (n+k)r_1x_2}{kn} & -mx_2 \\ 0 & r_2 + \mu mx_2 - \beta - e_2 \end{pmatrix}.$$

The eigenvalues of J_{E_2} are

$$\lambda_1 = \frac{-2r_1x_2^2 + (n+k)r_1x_2}{kn} = \frac{\left[r_1(k+n) - \sqrt{\Delta}\right]\sqrt{\Delta}}{2r_1kn} > 0, \quad \lambda_2 = r_2 + \mu m x_2 - \beta - e_2.$$

Thereby, if $e_2 < r_2 - \beta + \mu m x_2$, then $\lambda_2 > 0$, and E_2 is an unstable node or focus point; if $e_2 > r_2 - \beta + \mu m x_2$, then $\lambda_2 < 0$, and E_2 is an unstable saddle point. This completes the proof.

Next we will focus on the stability of the internal equilibrium point, then we have the following one theorem.

Theorem 3.2.4. Suppose $E_3(x_3, y_3)$ exists, then model (2.3) has a unique interal equilibrium point E_3. E_3 is locally asymptotically stable if $Tr(J_{E_3}) < 0$, and unstable if $Tr(J_{E_3}) > 0$.

Proof: The Jacobian matrix of the model (2.3) evaluated at E_3 is given by:

$$J_{E_3} = \begin{pmatrix} \dfrac{-2r_1x_3^2 + (n+k)r_1x_3}{kn} & -mx_3 \\ \mu m y_3 & 0 \end{pmatrix},$$

the expression of characteristic equations of $J_{E_3}(x_3, y_3)$ is

$$\lambda^2 - \left[\frac{-2r_1x_3^2 + (n+k)r_1x_3}{kn}\right]\lambda + \mu m^2 x_3 y_3 = 0.$$

And the determinant and the trace of matrix J_{E_3} are given by,

$$Tr(J_{E_3}) = \lambda_1 + \lambda_2 = \frac{-2r_1x_3^2 + (n+k)r_1x_3}{kn},$$

$$Det(J_{E_3}) = \lambda_1\lambda_2 = \mu m^2 x_3 y_3.$$

It is easy to check that $Det(J_{E_3})$ is always positive. Hence, if $Tr(J_{E_3}) < 0$, then E_3 is locally asymptotically stable; if $Tr(J_{E_3}) > 0$, then E_3 is unstable. If we substitute the expression of E_3 into the trace of the Jacobian matrix, we can't directly derive the sign of $Tr(J_{E_3})$ because of algebraic complexity of the expression of it. Therefore, we have calculated the values of $Tr(J_{E_3})$ by using numerical simulation in Section 5. This completes the proof.

3.3. Existence of Limit Cycle

In this subsection, E_3 is the unique internal equilibrium point, which is unstable. As for the model (2.3), we have the following main theorem about the existence of limit cycle.

Theorem 3.3.1. When the condition $r_2 < \beta + e_2$ is satisfied, there exists at least one limit cycle of the model (2.3).

Proof: Now we will prove Theorem 3.3.1 by constructing an invariant region Ω, which consists of the following line L_1, L_2, and x, y axis,

$$L_1 : x - \frac{r_1(k+n) + \sqrt{r_1^2(k+n)^2 - 4r_1kn(r_1+e_1)}}{2r_1} = 0, \quad L_2 : x + \frac{y}{\mu} - Q = 0.$$

Then, we have

$$\frac{dL_1}{dt} = \frac{dx}{dt} = \left[r_1 x \left(1 - \frac{x}{k}\right)\left(\frac{x}{n} - 1\right) - mxy - e_1 x \right]\Bigg|_{x = \frac{r_1(k+n) + \sqrt{r_1^2(k+n)^2 - 4r_1 kn(r_1 + e_1)}}{2r_1}} = -mxy < 0,$$

$$\frac{dL_2}{dt} = \frac{dx}{dt} + \frac{1}{\mu}\frac{dy}{dt} = \left[r_1 x \left(1 - \frac{x}{k}\right)\left(\frac{x}{n} - 1\right) - mxy - e_1 x + \frac{r_2 y}{\mu} + mxy - \frac{\beta y}{\mu} - \frac{e_2 y}{\mu} \right]\Bigg|_{y = \mu(Q - x)}$$

$$= r_1 x \left(1 - \frac{x}{k}\right)\left(\frac{x}{n} - 1\right) - e_1 x + (Q - x)\left[r_2 - \beta - e_2\right] < 0.$$

From the above equation, we can easily see that when $r_2 < \beta + e_2$ and Q is an adequately large constant, then $(Q - x)\left[r_2 - \beta - e_2\right]$ is a quite small negative number for any specific $x \in [n, k]$, meanwhile $r_1 x \left(1 - \frac{x}{k}\right)\left(\frac{x}{n} - 1\right) - e_1 x$ is bounded.

Thus, It is easy to verify that $\frac{dL_2}{dt} < 0$ for

$$0 < x < \frac{r_1(k+n) + \sqrt{r_1^2(k+n)^2 - 4r_1 kn(r_1 + e_1)}}{2r_1},$$ which means that the model (2.3) exists at least one limit cycle by Poincare-Bendixson Theorem [45] [46]. This ends the proof.

In order to make the results more visualized, we fix the parameters $r_1 = 0.6$, $n = 0.5$, $k = 2$, $m = 0.42857$, $r_2 = 0.2$, $\mu = 0.56$, $\beta = 0.5$, $e_1 = 0.2$, $e_2 = 0.2$, then E_3 is the unique equilibrium point of the model (2.3), which is unstable. At the same time, the condition $\frac{dL_2}{dt} < 0$ is satisfied when $Q = 2$, so it is obvious to find from **Figure 1** that there exists one limit cycle at least. The condition $\frac{dL_1}{dt} < 0$ means that the density values of the two populations will tend to the
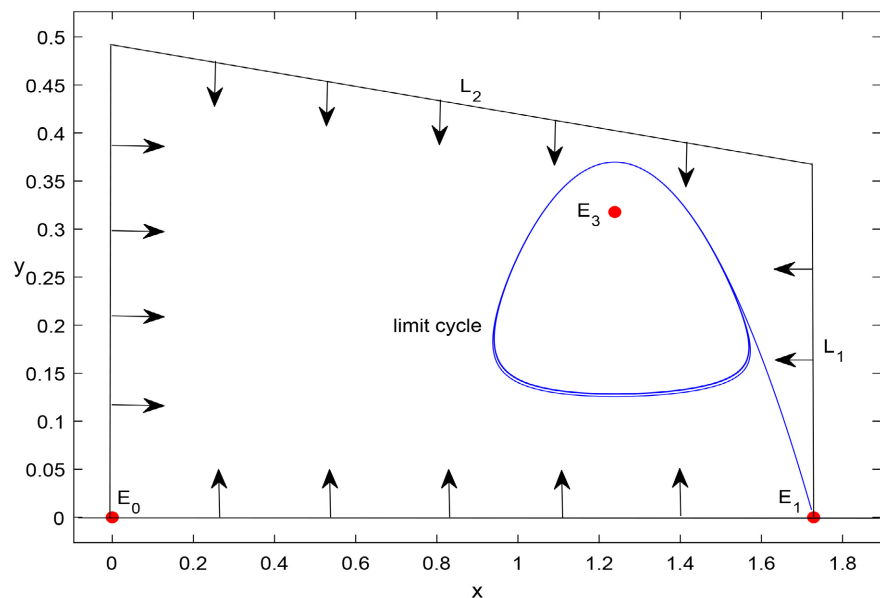

Figure 1. The existence of limit cycle with $r_1 = 0.6$, $n = 0.5$, $k = 2$, $m = 0.42857$, $r_2 = 0.2$, $\mu = 0.56$, $\beta = 0.5$, $e_1 = 0.2$, $e_2 = 0.2$, $Q = 2$, where E_3 is the unique internal equilibrium point in the region.

left side of the line L_1 when the density values lie on the line, $\dfrac{dL_2}{dt} < 0$ means that the density values of the two populations will tend to the down side of the line L_2 when the density values lie on the line. Furthermore, the limit cycle describes such a phenomenon in biology that neither of algae and fish will be extinct, but reach a state of periodic oscillation and dynamic coexistence.

4. Bifurcation Analysis

In this section, we will discuss possible bifurcation problems in model (2.3). The conditions for transcritical bifurcations and hopf bifurcations will be expressed mathematically and analyzed numerically.

4.1. Transcritical Bifurcation

Transcritical bifurcation usually occurs at the boundary equilibrium point. From Theorem 3.2.2, the boundary equilibrium point E_1 loses stability at
$e_2 = r_2 + \mu m x_1 - \beta$ and one eigenvalue of J_{E_1} is zero, indicating that the equilibrium point E_1 becomes non-hyperbolic. As the parameters change, it is possible for the model to occur transcritical bifurcation near E_1. In this subsection, we will show that the model (2.3) undergoes a transcritical bifurcation at E_1.

Theorem 4.1.1. The model (2.3) undergoes a transcritical bifurcation when $e_2 = e_{2TC}$, where $e_{2TC} = r_2 + \mu m x_1 - \beta$.

Proof: We use Sotomayor's theorem [47] [48] to prove that the model (2.3) undergoes a transcritical bifurcation. We consider e_2 as bifurcation parameter. As e_2 crosses e_{2TC} from left to right, E_1 will change from an unstable point to an stable point. When $e_2 = e_{2TC}$, the Jacobian matrix at E_1 can be expressed as

$$
J_{(E_1, w_{TC})} = \begin{pmatrix} \dfrac{-2r_1 x_1^2 + (n+k) r_1 x_1}{kn} & -m x_1 \\ 0 & 0 \end{pmatrix}.
$$

It is known that when $e_2 = e_{2TC}$, then $Det(J_{E_1}) = 0$. That means the Jacobian matrix J_{E_1} has at least one zero eigenvalue. Now, let V and W be the eigenvectors corresponding to the zero eigenvalue of J_{E_1} and $J_{E_1}^{\mathrm{T}}$ respectively. After a simple calculation they can be given by

$$
J_{E_1} \cdot V = 0 \cdot V, \, J_{E_1}^{\mathrm{T}} \cdot W = 0 \cdot W,
$$

We can set,

$$
V = \begin{pmatrix} v_1 \\ v_2 \end{pmatrix} = \begin{pmatrix} 0 \\ \dfrac{-2r_1 x_1 + (n+k) r_1}{kn} \end{pmatrix}, \quad W = \begin{pmatrix} w_1 \\ w_2 \end{pmatrix} = \begin{pmatrix} 0 \\ 1 \end{pmatrix},
$$

Due to

$$
F_{e_2}(E_1, e_{2TC}) = \begin{pmatrix} F_{1e_2} \\ F_{2e_2} \end{pmatrix} = \begin{pmatrix} 0 \\ -y_1 \end{pmatrix}_{(E_1, e_{2TC})} = \begin{pmatrix} 0 \\ 0 \end{pmatrix},
$$

$$DF_{e_2}(E_1, e_{2TC})V = \begin{pmatrix} F_{1e_2x} & F_{1e_2y} \\ F_{2e_2x} & F_{2e_2y} \end{pmatrix} \begin{pmatrix} v_1 \\ v_2 \end{pmatrix}$$

$$= \begin{pmatrix} 0 & 0 \\ 0 & -1 \end{pmatrix}_{(E_1, e_{2TC})} \begin{pmatrix} m \\ \dfrac{-2r_1x_1 + (n+k)r_1}{kn} \end{pmatrix}$$

$$= \begin{pmatrix} 0 \\ \dfrac{2r_1x_1 - (n+k)r_1}{ukn} \end{pmatrix},$$

$$D^2F(E_1, e_{2TC})(V,V) = \begin{pmatrix} F_{1xx} & F_{1xy} & F_{1yx} & F_{1yy} \\ F_{2xx} & F_{2xy} & F_{2yx} & F_{2yy} \end{pmatrix}_{(E_1, e_{2TC})} \begin{pmatrix} v_1v_1 \\ v_1v_2 \\ v_2v_1 \\ v_2v_2 \end{pmatrix}$$

$$= \begin{pmatrix} \dfrac{(-4x_1+n+k)r_1}{kn} & -m & -m & 0 \\ 0 & \mu m & \mu m & 0 \end{pmatrix} \begin{pmatrix} m^2 \\ \dfrac{(-2x_1+n+k)r_1m}{kn} \\ \dfrac{(-2x_1+n+k)r_1m}{kn} \\ \dfrac{(-2x_1+n+k)^2 r_1^2}{k^2n^2} \end{pmatrix}$$

$$= \begin{pmatrix} \dfrac{-(n+k)r_1m^2}{kn} \\ \dfrac{\mu m^2 r_1[-4x_1 + 2(n+k)]}{kn} \end{pmatrix}.$$

Furthermore, we can obtain

$$W^{\mathrm{T}} \cdot F_{e_2}(E_1, e_{2TC}) = \begin{pmatrix} 0 & 1 \end{pmatrix} \begin{pmatrix} 0 \\ 0 \end{pmatrix} = 0,$$

$$W^{\mathrm{T}}\left[DF_{e_2}(E_1, e_{2TC})V\right] = \begin{pmatrix} 0 & 1 \end{pmatrix} \begin{pmatrix} 0 \\ \dfrac{2r_1x_1 - (n+k)r_1}{kn} \end{pmatrix}$$

$$= \frac{2r_1x_1 - (n+k)r_1}{kn} = \frac{r_1(k+n)\sqrt{\Delta} + \Delta^2}{2r_1kn} \neq 0,$$

$$W^{\mathrm{T}}\left[D^2F(E_1, e_{2TC})(V,V)\right] = \begin{pmatrix} 0 & 1 \end{pmatrix} \begin{pmatrix} \dfrac{-(n+k)r_1m^2}{kn} \\ \dfrac{\mu r_1m^2(-4x_1 + 2n + 2k)}{kn} \end{pmatrix}$$

$$= \frac{2\mu r_1m^2(-2x_1 + n + k)}{kn} \neq 0.$$

Thus, from Sotomayor's theorem we can deduce that the model (2.3) undergoes a transcritical bifurcation as e_2 passes through threshold $e_2 = e_{2TC}$. This completes the proof.

Similar to the above theorem, the following two theorems can be obtained.

Theorem 4.1.2. The model (2.3) undergoes a transcritical bifurcation when

$$e_1 = e_{1TC}, \text{ where } r_2 + \mu m \left(\frac{r_1(k+n) + \sqrt{r_1^2(k+n)^2 - 4r_1kn(r_1 + e_{1TC})}}{2r_1} \right) - \beta - e_2 = 0.$$

Theorem 4.1.3. The model (2.3) undergoes a transcritical bifurcation when

$$m = m_{TC}, \text{ where } m_{TC} = \frac{e_2 + \beta - r_2}{\mu x_1}.$$

4.2. Hopf Bifurcation

The equilibrium point $E_3(x_3, y_3)$ has different stability under different restrictions of parameters, which may caused by Hopf bifurcation. In order to figure out how harvesting effort, the proportion of prey captured by predators and Allee effect influence the dynamic behavior of the model (2.3), e_2, m and n are chosen as the control parameter of Hopf bifurcation respectively, then we have the following three Theorems. Next, we discuss the Hopf bifurcation of the model (2.3) at the positive equilibrium point $E_3 = (x_3, y_3)$, where

$$x_3 = \frac{\beta + e_2 - r_2}{\mu m}, y_3 = \frac{r_1\left(1 - \frac{x_3}{k}\right)\left(\frac{x_3}{n} - 1\right) - e_1}{m}.$$

Theorem 4.2.1. Based on the Theorem 3.2.4, the model (2.3) undergoes a Hopf bifurcation around E_3 at $e_2 = e_{2Hp}$.

Proof: As for matrix J_{E_3}, the characteristic equation of it can be written as $\lambda^2 - Tr(J_{E_3})\lambda + Det(J_{E_3}) = 0$, then Hopf bifurcation takes place when $e_2 = e_{2Hp}$ such that

1) $Tr(J_{E_3}) = 0$,
2) $Det(J_{E_3}) > 0$,
3) $\left.\frac{\mathrm{d}}{\mathrm{d}e_2}Tr(J_{E_3})\right|_{e_2 = e_{2Hp}} \neq 0$.

We've already proved $Det(J_{E_3}) > 0$. And when $e_2 = e_{2Hp}$, $Tr(J_{E_3}) = 0$ is set up. Therefore, the characteristic equation of E_3 has two pure imaginary roots $\lambda_{(1,2)}(e_{2HP}) = \pm i\omega(e_{2HP})$. So we only need to certify the transersality condition (3) to guarantee the changes of stability of E_3 through Hopf bifurcation.

$$\left.\frac{\mathrm{d}}{\mathrm{d}e_2}Tr(J_{E_3})\right|_{e_2 = e_{2Hp}} = \left[\frac{-4r_1x_3 + (n+k)r_1}{kn}\frac{\mathrm{d}x_3}{\mathrm{d}e_2}\right]_{e_2 = e_{2Hp}}$$

$$= \left[\frac{r_1(-4\beta - 4e_2 + 4r_2 + n\mu m + k\mu m)}{kn\mu^2 m^2}\right]_{e_2 = e_{2Hp}}.$$

The condition (3) is satisfied through our numerical simulation, then Hopf bifurcation takes place in the model (2.3) at $e_2 = e_{2Hp}$.

To find out the stability of the limit cycle brought by Hopf bifurcation, the first Lyapunov number l_1 at the equilibrium point E_3 is going to be computed following. The fixed parameter e_2 is at its critical value e_{2Hp}, when the coordi-

nates of the internal equilibrium point E_3 are $\left(x_3 \big|_{e_2 = e_{2Hp}}, y_3 \big|_{e_2 = e_{2Hp}} \right)$. Doing varia-
ble transformation

$$
\begin{cases}
x = x_{e_2} + x_3 \big|_{e_2 = e_{2Hp}}, \\
y = y_{e_2} + y_3 \big|_{e_2 = e_{2Hp}},
\end{cases}
$$

and for Taylor to expand, then the model (2.3) can be rewritten as

$$
\begin{cases}
\dot{x}_{e_2} = \alpha_{10} x_{e_2} + \alpha_{01} y_{e_2} + \alpha_{20} x_{e_2}^2 + \alpha_{11} x_{e_2} y_{e_2} + \alpha_{02} y_{e_2}^2 + \alpha_{30} x_{e_2}^3 \\
\qquad + \alpha_{21} x_{e_2}^2 y_{e_2} + \alpha_{12} x_{e_2} y_{e_2}^2 + \alpha_{03} y_{e_2}^3 + P\left(x_{e_2}, y_{e_2} \right), \\
\dot{y}_{e_2} = \beta_{10} x_{e_2} + \beta_{01} y_{e_2} + \beta_{20} x_{e_2}^2 + \beta_{11} x_{e_2} y_{e_2} + \beta_{02} y_{e_2}^2 + \beta_{30} x_{e_2}^3 \\
\qquad + \beta_{21} x_{e_2}^2 y_{e_2} + \beta_{12} x_{e_2} y_{e_2}^2 + \beta_{03} y_{e_2}^3 + R\left(x_{e_2}, y_{e_2} \right),
\end{cases}
$$

where

$$
\alpha_{10} = \frac{-2r_1 x_3^2 + (n+k) r_1 x_3}{kn}, \quad \alpha_{20} = \frac{-4r_1 x_3 + (n+k) r_1}{kn}, \quad \alpha_{30} = \frac{-4r_1}{kn},
$$
$$
\alpha_{01} = -m x_3, \quad \alpha_{11} = -m, \quad \alpha_{02} = \alpha_{03} = \alpha_{21} = \alpha_{12} = 0,
$$

and

$$
\beta_{10} = \mu m y_3, \quad \beta_{01} = r_2 + \mu m x_3 - \beta - e_2, \quad \beta_{11} = \mu m,
$$
$$
\beta_{02} = \beta_{20} = \beta_{30} = \beta_{03} = \beta_{21} = \beta_{12} = 0,
$$

and $P\left(x_{e_2}, y_{e_2} \right), R\left(x_{e_2}, y_{e_2} \right)$ are power series with terms $x_{e_2}^i y_{e_2}^j \ (i+j \geq 4)$.

The expression of the first Lyapunov number can be expressed by the formula:

$$
\begin{aligned}
l_1 = \frac{-3\pi}{2\alpha_{01}\Delta^{3/2}} & \left\{ \left[\alpha_{10}\beta_{10}\left(\alpha_{11}^2 + \alpha_{11}\beta_{02} + \alpha_{02}\beta_{11} \right) + \alpha_{10}\alpha_{01}\left(\beta_{11}^2 + \alpha_{20}\beta_{11} + \alpha_{11}\beta_{02} \right) \right. \right. \\
& + \beta_{10}^2 \left(\alpha_{11}\alpha_{02} + 2\alpha_{02}\beta_{02} \right) - 2\alpha_{10}\beta_{10}\left(\beta_{02}^2 - \alpha_{20}\alpha_{02} \right) - 2\alpha_{10}\alpha_{01}\left(\alpha_{20}^2 - \beta_{20}\beta_{02} \right) \\
& \left. - \alpha_{01}^2 \left(2\alpha_{20}\beta_{20} + \beta_{11}\beta_{20} \right) + \left(\alpha_{01}\beta_{10} - 2\alpha_{10}^2 \right)\left(\beta_{11}\beta_{02} - \alpha_{11}\alpha_{20} \right) \right] - \left(\alpha_{10}^2 + \alpha_{01}\beta_{10} \right) \\
& \left. \times \left[3\left(\beta_{10}\beta_{03} - \alpha_{01}\alpha_{30} \right) + 2\alpha_{10}\left(\alpha_{21} + \beta_{12} \right) + \left(\beta_{10}\alpha_{12} - \alpha_{01}\beta_{21} \right) \right] \right\}
\end{aligned}
$$

where

$$
\Delta = \alpha_{10}\beta_{01} - \alpha_{01}\beta_{10} > 0.
$$

If $l_1 < 0$, the limit cycle is stable; if $l_1 > 0$, the limit cycle is unstable. However, the expression for Lyapunov number l_1 is rather cumbersome, we cannot directly judge the sign of it, so we will give some numerical simulation results in Section 5.

Similar to the above theorem, the following two theorems can be obtained.

Theorem 4.2.2. Based on the Theorem 3.2.4, the model (2.3) undergoes a Hopf bifurcation around E_3 at $m = m_{Hp}$.

Theorem 4.2.3. Based on the Theorem 3.2.4, the model (2.3) undergoes a Hopf bifurcation around E_3 at $n = n_{Hp}$.

5. Numerical Simulations

In Sections 2, 3 of the article, we have obtained some theoretical results of the

model (2.3) through analysis and mathematical proofs, but due to the complexity of some expressions in the theoretical derivation process, in order to verify the feasibility and validity of the theoretical results, and to more intuitively understand the dynamic behavior of the model (2.3). So as to explore how harvesting term, Allee effect, and predator capture rate affect the dynamics between algae and fish, we will perform some precise numerical simulations in this section. In the numerical simulations, we consider a set of hypothetical values of $r_1 = 0.6$, $k = 2$, $r_2 = 0.2$, $\mu = 0.56$, and $\beta = 0.5$ based on the biological significance of parameters in the model (2.3).

In order to better investigate the effects of harvesting term and predator capture rate on model (2.3), we let the parameters e_2 and m vary within a certain range, respectively, under the premise of fixing the other parameters above, and obtain the phase and bifurcation diagrams when e_2 and m are varied, as shown in **Figure 2**. It is obvious from the two diagrams in **Figure 2** that the model (2.3) has rich dynamic properties. When $e_2 = e_{2Hp} = 0.11$, $m = m_{Hp} = 0.428571428$, the model (2.3) occurs Hopf bifurcation; when $e_2 = e_{2TC} = 0.1904$, $m = m_{TC} = 0.309891875$, the model (2.3) occurs transcritical bifurcation. The two vertical lines in **Figure 2** are the Hopf bifurcation line and the transcritical bifurcation line, representing Hp and TC, respectively.

First, the model (2.3) has an internal positive equilibrium point E_3 when $e_2 = 0.109 < e_{2Hp} = 0.11$. Since $Tr(J_{E_3}) > 0$, $Det(J_{E_3}) > 0$, the Jacobian matrix corresponding to the equilibrium point E_3 has two eigenvalues greater than 0, hence E_3 is an unstable focus point. Moreover, from **Figure 3(a)**, we can observe that there is a limit cycle in the small neighborhood containing E_3, which is caused
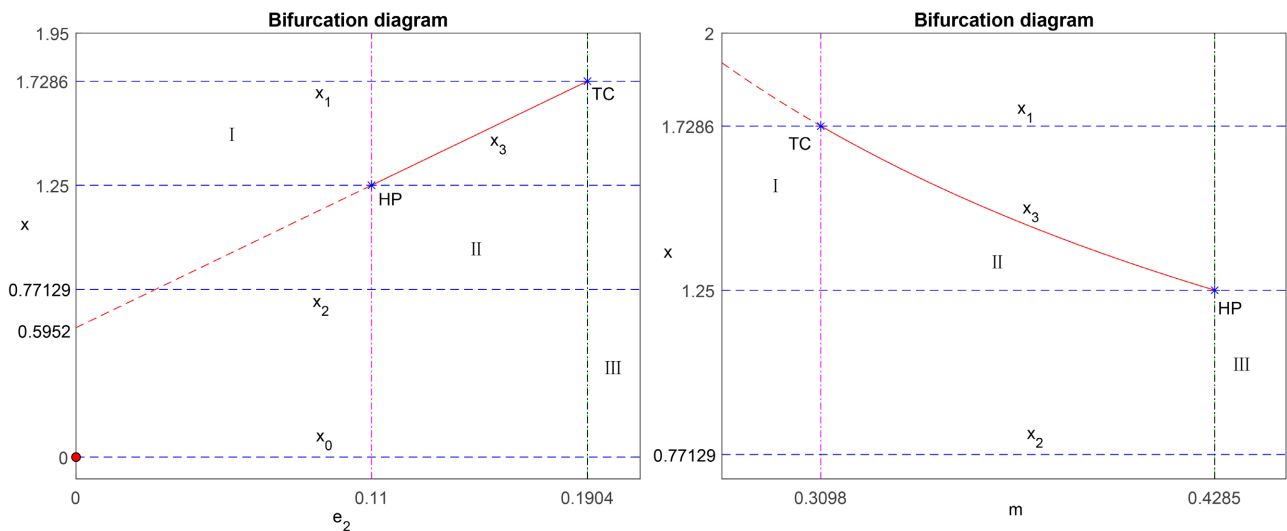

Figure 2. Bifurcation diagram of the model (2.3) by taking e_2 and m as bifurcation parameter respectively. Here, Bifurcation diagram with respect to parameter $e_{2HP} = 0.11$, $e_{2TC} = 0.1904$ and $m_{HP} = 0.428571428$, $m_{TC} = 0.309891875$. Moreover, the vertical lines with labels "Hp" and "TC" indicate that the model (2.3) undergoes Hopf and transcritical bifurcation here respectively. The red curves represent the internal equilibrium point E_3. Equilibrium point presented as solid curves are stable, dotted curves are unstable. In addition, blue asterisks denote the bifurcation points of Hopf bifurcation and transcritical bifurcation, respectively. This paper makes a detailed analysis of it.
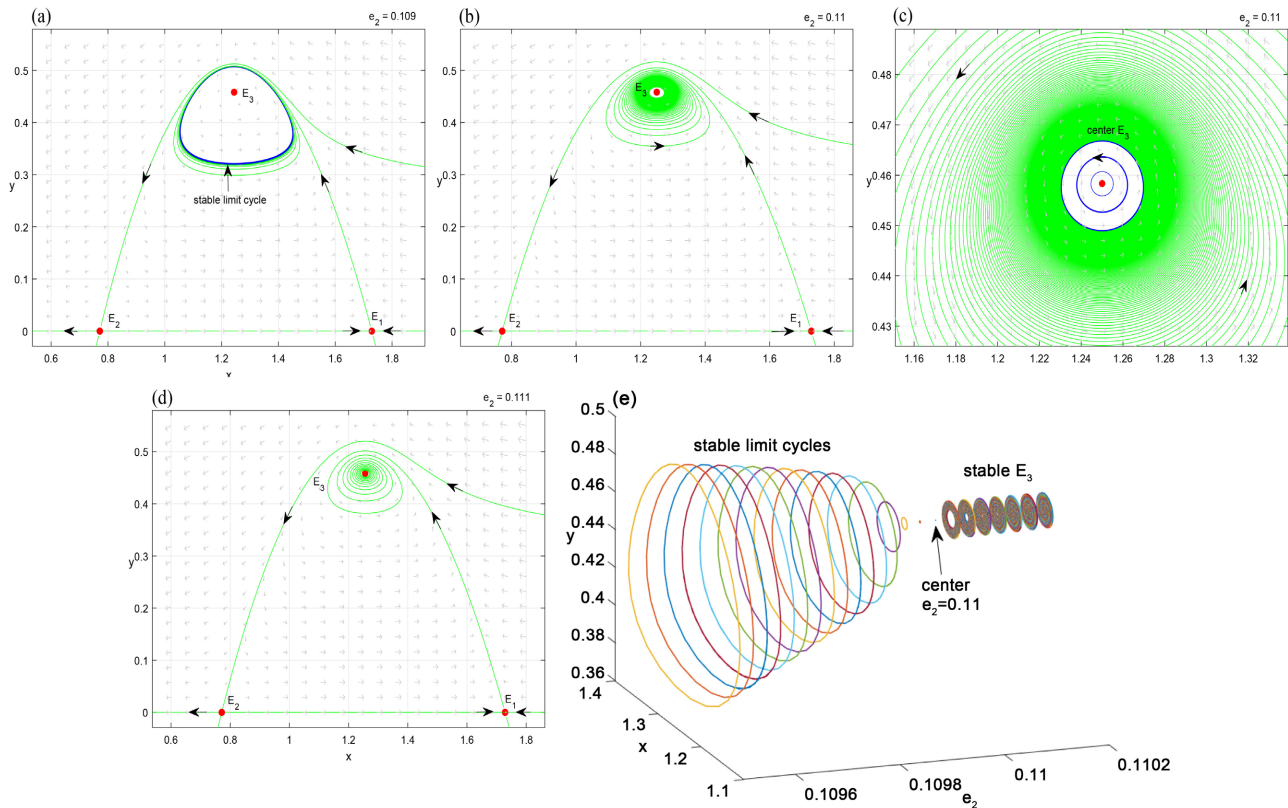
Figure 3. The phase portraits of the model (2.3) where E_3 has different dynamics (varying with parameter e_2). (a) When $e_2 = 0.109 < e_{2HP}$, E_3 is an unstable focus or node point. (b) When $e_2 = 0.11 = e_{2HP}$, E_3 yields a periodic solution via Hopf bifurcation. (c) Local enlargement of (b), where $(x, y) \in [1.245, 0.45] \times [1.255, 0.5]$. (d) Through Hopf bifurcation with $e_2 = 0.111 > e_{2HP}$, there exists a stable periodic orbits around the stable focus point E_3. (e) Hopf bifurcation diagram representing stable E_3 and stable limit cycles with various values of e_2.

by the unstable trajectory of the saddle point E_1. At the same time, we can compute the first Lyapunov number $l_{e_2} = -52.9641\pi < 0$, which implies that the limit cycle is stable. Therefore, the model (2.3) has an internal equilibrium point E_3 when the value of e_2 becomes larger and larger, reaching $e_{2Hp} = 0.11$.

$Tr(J_{E_3}) = 0$, $Det(J_{E_3}) > 0$, E_3 becomes the center from the unstable focus point, a stable limit cycle appears. The supercritical Hopf bifurcation occurs, whereby the population densities are in a certain range and the algal-fish coexist in the equilibrium point E_3. When $e_2 = 0.111 > e_{2Hp} = 0.11$, the model (2.3) has an internal equilibrium point E_3. Since $Tr(J_{E_3}) < 0$, $Det(J_{E_3}) > 0$, so that the Jacobian matrix corresponding to E_3 has two eigenvalues less than 0. At this point, E_3 is a stable focus point. There will be a gradual formation of coexistence mode of cyclic oscillations between algae and fish. Within a certain small range, the larger the value of e_2, the more favorable the coexistence of periodic oscillation between algae and fish. Meanwhile, the boundary equilibrium points E_1 and E_2 are always unstable saddle points, and the extinction equilibrium point E_0 is always a stable node point. In addition, from the numerical simulation results, we found that the value of the harvesting parameter e_2 seriously affects the dynamic behavior of

the model (2.3). The detailed dynamic evolution of the Hopf bifurcation with e_2 as the parameter is shown in **Figure 3**.

Previously, we analyzed the effect of the harvesting parameter e_2 on the Hopf bifurcation in the model (2.3). In the following we will discuss the effect of the predator capture rate parameter m on the Hopf bifurcation in the model (2.3). When $m = 0.426 < m_{Hp} = 0.428571428$, the model (2.3) has an internal positive equilibrium point E_3. Since $Tr(J_{E_3}) < 0$, $Det(J_{E_3}) > 0$, the Jacobian matrix corresponding to the equilibrium point E_3 has two eigenvalues less than 0, so E_3 is a stable focus point. However, when the value of m becomes larger and larger and reaches $m_{Hp} = 0.428571428$, at this time E_3 changes from a stable focus to a center, and there is a stable limit cycle. At the same time, we can calculate that the first Lyapunov number $l_m = -44.3129\pi < 0$, which implies that the limit cycle is stable. However, when $m = 0.43 > m_{Hp} = 0.428571428$, at this point $Tr(J_{E_3}) > 0$, $Det(J_{E_3}) > 0$, E_3 is an unstable focus point. From **Figure 4(c)**, we can observe that there exists a limit cycle in the small neighborhood containing E_3, which is caused by the unstable trajectory of the saddle point E_1. From **Figure 4(d)**, it can be observed that the coexistence mode of periodic oscillation in algae
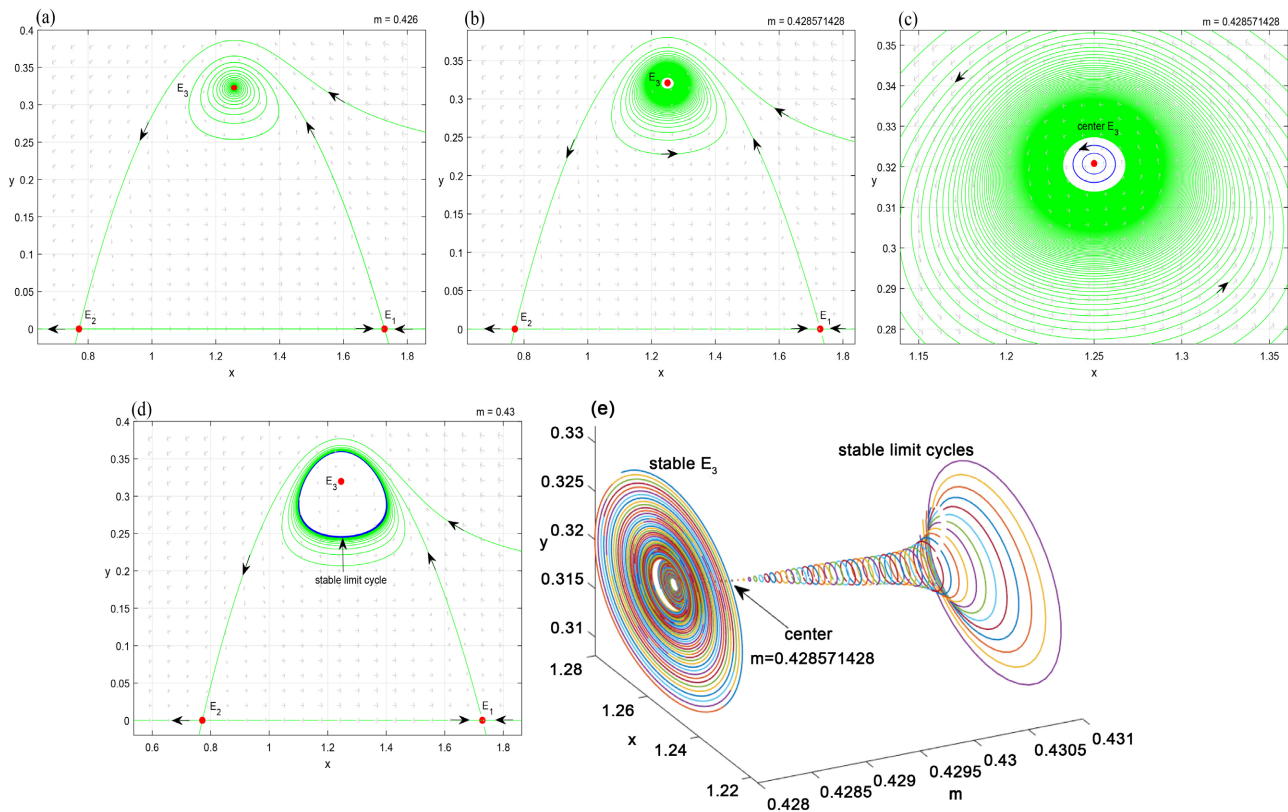

Figure 4. The phase portraits of the model (2.3) where E_3 has different dynamics (varying with parameter m). (a) When $m = 0.426 < m_{HP}$, there exists a stable periodic orbits around the stable focus point E_3. (b) When $m = 0.428571428 = m_{HP}$, E_3 yields a periodic solution via Hopf bifurcation. (c) Local enlargement of (c), where $(x, y) \in [1.245, 0.31] \times [1.255, 0.33]$. (d) Through Hopf bifurcation with $m = 0.43 > m_{HP}$, E_3 is an unstable focus or node point. (e) Hopf bifurcation diagram representing stable E_3 and stable limit cycles with various values of m.

and fish at this time is formed. It is also worth emphasizing that the amplitude of the limit cycles decreases with increasing values of m. Which implies that the smaller the effect of the predator capture rate on the algae and fish, the wider the area in which the periodic oscillations between algae and fish coexist. Over time, filter-feeding fish and algae eventually reach a state of coexistence within a small range of $m < m_{Hp}$.

In order to investigate the effect of Allee effect in the model (2.3), we chose Allee effect parameter n for Hopf bifurcation. After numerical simulations, we found that the effect of Allee effect in the model is similar to that of the predator capture rate m on the prey. When $n = 0.14 < n_{Hp} = 0.14285714$, E_3 is a stable focus point, the algae and fish form a coexistence mode of periodic oscillations. However, when the value of n becomes larger and larger and reaches n_{Hp}, then E_3 changes from a stable focus to a center. There is a stable limit cycle, and supercritical Hopf bifurcation occurs. At the same time, we can calculate the first Lyapunov number $l_n = -45.3149\pi < 0$, which means that the limit cycle is stable. However, when $n = 0.148 > n_{Hp} = 0.14285714$, E_3 is an unstable focus point. From **Figure 5(c)**, we can observe that there exists a limit cycle in the small
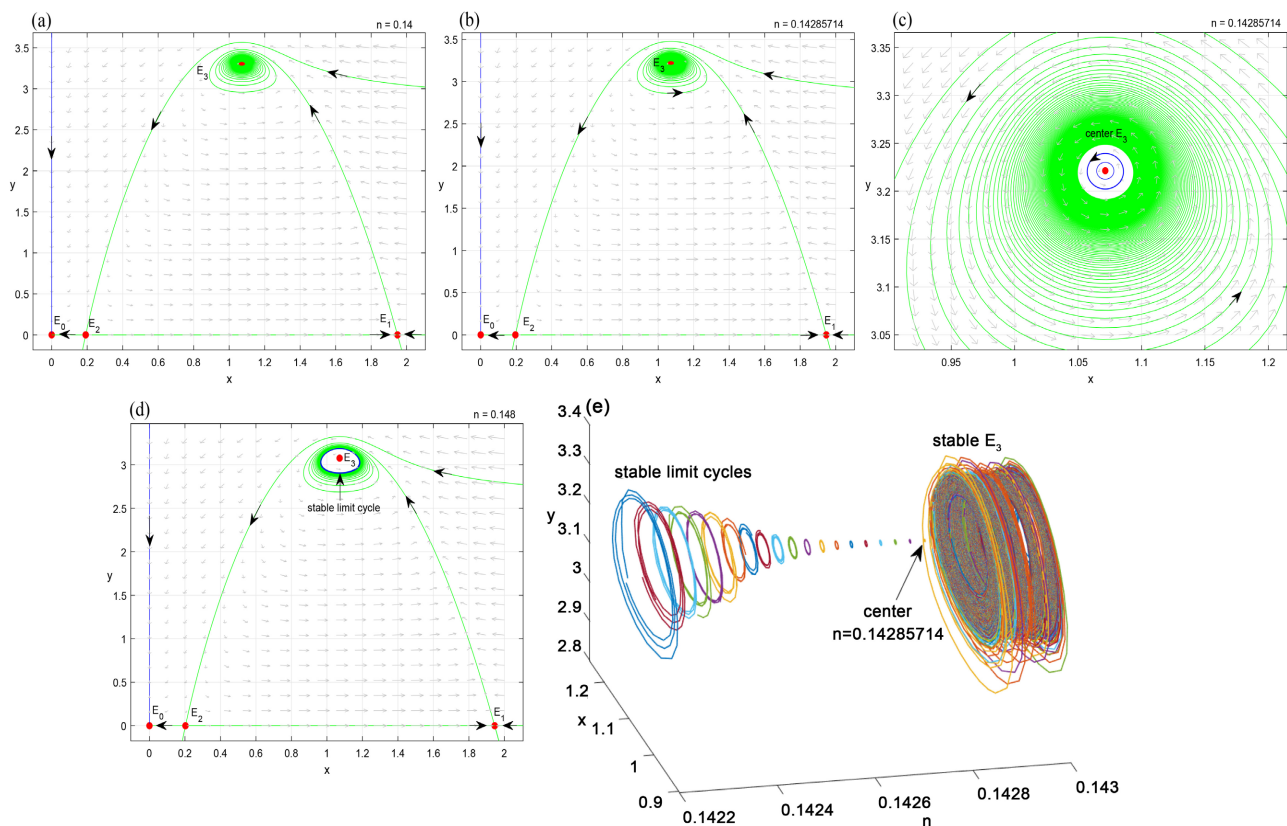

Figure 5. The phase portraits of the model (2.3) where E_3 has different dynamics (varying with parameter n). (a) When $n = 0.14 < n_{HP}$, there exists a stable periodic orbits around the stable focus point E_3. (b) When $n = 0.14285714 = n_{HP}$, E_3 yields a periodic solution via Hopf bifurcation. (c) Local enlargement of (c), where $(x, y) \in [1.01, 3.2] \times [1.1, 3.3]$. (d) Through Hopf bifurcation with $n = 0.148 > n_{HP}$, E_3 is an unstable focus or node point. (e) Hopf bifurcation diagram representing stable E_3 and stable limit cycles with various values of m.

neighborhood containing E_3, which is caused by the unstable trajectory of the saddle point E_1. In addition, it is worth emphasizing that the amplitude of the limit cycle decreases with the increase of the n value, which means that the less Allee effect affects algae and fish in a certain range, the wider the area of coexistence of periodic oscillations between algae and fish.

The stability switching across the transcritical bifurcation can be better explained by the phase diagrams in **Figures 6-8**. When the model (2.3) undergoes a transcritical bifurcation, harvesting parameters e_2 and e_1 have the same dynamic effects on it. When $e_2 = 0.16 < e_{2TC}$ and $e_1 = 0.13 < e_{1TC}$, the system (2.3) has an internal positive equilibrium point E_3 which is a stable focus since $Tr(J_{E_3}) < 0$, $Det(J_{E_3}) > 0$. And the equilibrium point $E_1(1.7286, 0)$ is an unstable saddle point. The Jacobian matrix corresponding to the equilibrium point E_3 has two eigenvalues less than zero. When e_2 and e_1 increase to $e_{2TC} = 0.1904$ and $e_{1TC} = 0.1653$, respectively, there is a transcritical bifurcation occurs when the E_1 and E_3 vector fields overlap and E_1 collides with E_3, prompting saddle point E_1 to regain stability and return to the node. When $e_2 = 0.2 > e_{2TC}$ and
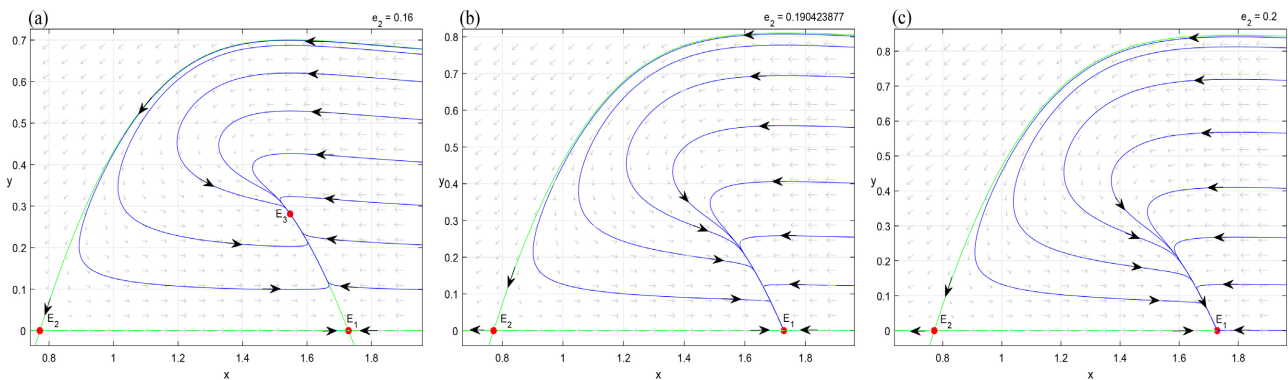

Figure 6. The phase portraits of the model (2.3) where E_3 has different dynamics (varying with parameter e_2). (a) When $e_2 = 0.16 < e_{2TC}$, E_3 is a node point, and E_1 is a saddle point. (b) The vector field graph for $e_2 = 0.1904 = e_{2TC}$ with point E_1 and point E_3 that coincide. (c) When $e_2 = 0.2 > e_{2TC}$, E_3 does not exist, and E_1 is a node point.
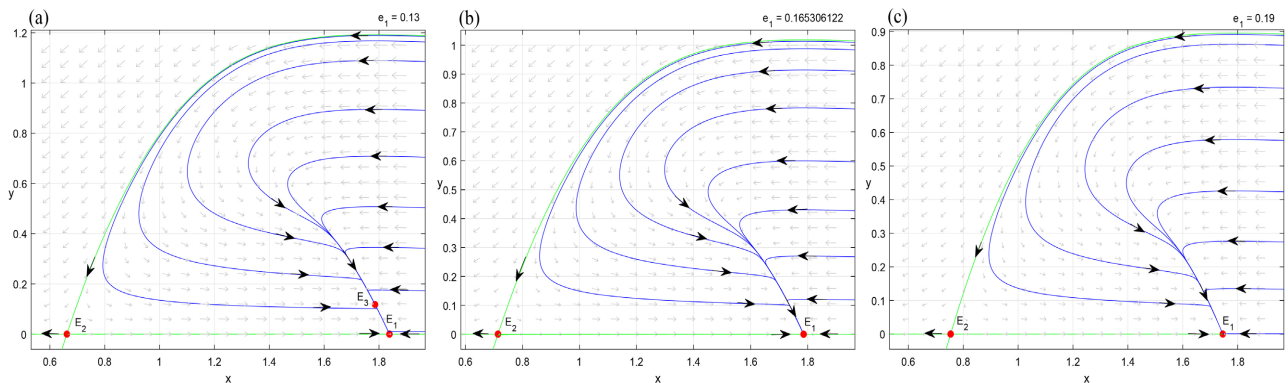

Figure 7. The phase portraits of the model (2.3) where E_3 has different dynamics (varying with parameter e_1). (a) When $e_1 = 0.13 < e_{1TC}$, E_3 is a node point, and E_1 is a saddle point. (b) The vector field graph for $e_1 = 0.165306122 = e_{1TC}$ with point E_1 and point E_3 that coincide. (c) When $e_1 = 0.19 > e_{1TC}$, E_3 does not exist, and E_1 is a node point.
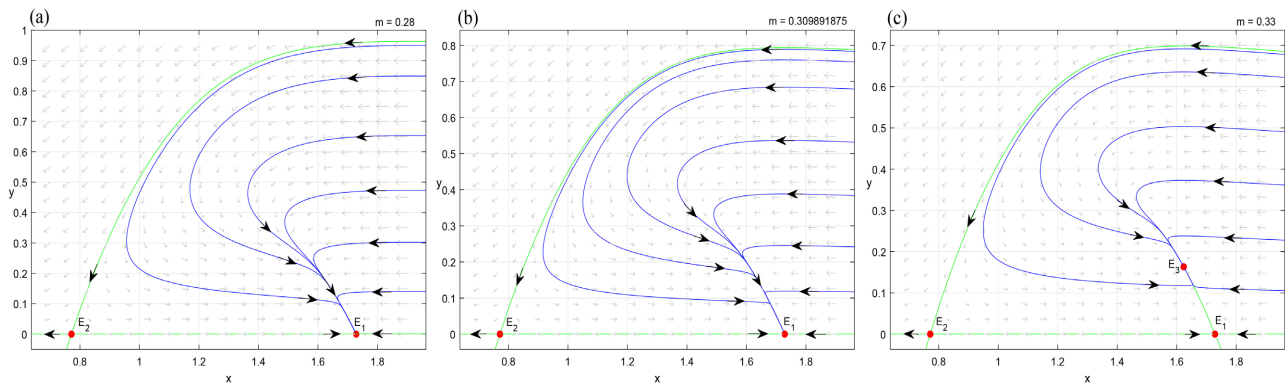
Figure 8. The phase portraits of the model (2.3) where E_3 has different dynamics (varying with parameter m). (a) When $m = 0.28 < m_{TC}$, E_1 is a node point and E_3 does not exist. (b) The vector field graph for $m = 0.309891875 = m_{TC}$ with point E_1 and point E_3 that coincide. (c) When $m = 0.33 > m_{TC}$, the boundary equilibrium E_1 separates the internal equilibrium E_3, E_3 is a node point and E_1 is a saddle point.

$e_1 = 0.19 > e_{1TC}$, the system (2.3) has no internal equilibrium point and the boundary equilibrium point E_1 remains stable. This suggests that filter-feeding fish become extinct when the initial density of algae exceeds a critical threshold. However, when the densities of algae and filter-feeding fish are within a certain range, they can coexist in a stable equilibrium point.

The effect of predator capture rate on the dynamical properties of model (2.3) is different from the harvesting parameters e_2 and e_1. It can be observed from the phase diagram in **Figure 8** that when $m = 0.28 < m_{TC} = 0.309891875$, the model has no internal equilibrium point at this point and the boundary equilibrium point E_1 is a stable node. When m increases to m_{TC}, the transcritical bifurcation occurs, which can prompt the node E_1 to become unstable as a saddle point and E_1 overlaps with the E_3 vector field. When $m = 0.33 > m_{TC}$, the model (2.3) has a stable internal equilibrium point E_3 and the boundary equilibrium point E_1 remains unstable. This suggests that algae and fish can coexist in a stable equilibrium point when the predator capture rate of the prey reaches a certain threshold.

From the above numerical simulation analysis, it can be seen that the values of the key parameters e_2, e_1, n and m have an important influence on the dynamic behavior of the model (2.3). Which can not only change the dynamic characteristics essentially, but also affect the survival and extinction of algae and fish. From **Figures 2-5**, it can be seen that the values of the key parameters e_2, n and m are very important for the occurrence of the Hopf bifurcation. Which not only relates to the long-term survival of algae and fish, but also leads to the formation of a stable coexistence mode of cyclic oscillations between algae and fish. It is clear from **Figures 6-8** that the values of the key parameters e_2, e_1, and m can lead to transcritical bifurcations, which are related to the range of densities at which algae and fish coexist and the critical threshold for extinction of fish. In summary, the harvesting term and Allee effect need to be considered when modeling aquatic ecology to further determine the dynamics between algae and fish.

6. Conclusions

In this paper, we propose an algae and fish ecological model with two harvesting terms and Allee effect based on the classical predator-prey model. Firstly, the existence of the equilibrium point is determined by analyzing the model (2.3). Secondly, the properties of the roots of the characteristic equation of the Jacobian matrix corresponding to the equilibrium point are analyzed, and the local stability of the equilibrium point is discussed, which also provides a theoretical basis for the subsequent discussion of the bifurcation dynamics. The results show that the internal equilibrium point can be a saddle point, a stable node or an unstable node when the model (2.3) takes different parameter values. Thirdly, the harvesting parameters e_2 and e_1, the predator capture rate m and Allee effect parameter n are selected as the bifurcation parameters, in order to theoretically derive the key threshold conditions that allow the model (2.3) to undergo transcritical bifurcation and Hopf bifurcation. At the same time, a rigorous mathematical proof of the existence of transcritical bifurcation is given using Sotomayor's theorem. Finally, the stability of the limit cycle of Hopf bifurcation is determined by calculating the first Lyapunov number, and a numerical simulation result is given.

In the numerical simulation part, the bifurcation theory analysis of the model (2.3) is further enriched by specific numerical examples and corresponding biological explanations. It is found that human harvesting effort on algae and fish has a significant effect on the dynamic survival mode of algae and fish populations. In addition, we found that fish eventually become extinct when harvesting effort is too high and exceeds a certain threshold, implying that aquatic ecological resource managers need to develop rational harvesting strategies. Only by adopting appropriate intensity of harvesting effort can the development of both populations be promoted to achieve the desired goal. Meanwhile, we observed that filter-feeding fish were extinct when their capture rate of algae was too low. And filter-feeding fish could coexist with algae only when the capture rate exceeded a certain threshold. The result suggests that in the early stage of algae population growth, a certain number of fish need to be released to effectively control algal blooms.

In subsequent research work, we need to make further modifications to the model to make it more suitable in real ecosystems. In fact, from several perspectives, including biological and economic, nonlinear harvesting is more relevant than constant and linear harvesting, due to the fact that harvesting does not always occur at constant yield or constant effort, and thus it is essential to consider nonlinear harvesting in algae and fish model, and we will continue to deepen it in our subsequent research.

Conflicts of Interest

The authors declare no conflicts of interest regarding the publication of this paper.

References

[1] Jia, Y., Schmid, C., *et al.* (2019) Toxicological and Ecotoxicological Evaluation of the Water Quality in a Large and Eutrophic Freshwater Lake of China. *Science of the Total Environment*, **667**, 809-820.

[2] Zhan, X.S. and Wang, L.P. (2019) The Study on Purification of Large Water Surface Water by Filter-feeding Fish. *Henan Fisheries*, **4**, 37-39.

[3] Song, H.L., Lu, X.W. and Inamori, Y. (2004) Pilot Investigation on Aquatic-Plant bed System Pre-Treating Eutrophicated Source Water. *Water & Wastewater Engineering*, **30**, 8-12.

[4] Li, R.H., Guan, Y.T., He, M., Hu, H.Y. and Jiang, Z.P. (2006) Pilot-Scale Study on Riparian Phragmites Communis, Zizania latifolia and Typha angustifolia L. Zones Treating Polluted River Water. *Environmental Science*, **27**, 493-497.

[5] Zhang, R.S., Li, G.H., Qi, Z. and Xu, Z. (2005) Effects of Plants on Nitrogen/Phosphorus Removal in Subsurface Constructed Wetlands. *Enviromental Science*, **26**, 83-86.

[6] Shapiro, J., Lamarra, V. and Lynch, M. (1975) Biomanipulation: An Ecosystem Approach to Lake Restoration. In: Brezonik P. and Fox, L., Eds., *Proceedings of a Symposium on Water Quality Management through Biological Control*, University Press of Florida, Gainesville, 85-96.

[7] Hansson, L., Annadotter, H., Bergman, E., *et al.* (1998) Biomanipulation as an Application of Food Chain Theory Constraints, Synthesis, and Recommendations for Temperate Lakes. *Ecosystems*, **1**, 558-574. https://doi.org/10.1007/s100219900051

[8] Ke, N. (2006) The Basic Concepts of Bio-Manipulation Technology. *Modern Fisheries Information*, **21**, 30.

[9] Perrow, M.R., Meijer, M., Dawidowicz, P., *et al.* (l997) Bio-Manipulation in Shallow Lake: State of the Art. *Hydrobiologia*, **342**, 355-356. https://doi.org/10.1023/A:1017092802529

[10] Liu, J.K. and Xie, P. (2003) Direct Control of Microcystis Bloom through the Use of Planktivorous Carp-Closure Experiments and Lake Fishery Practice. *Ecologic Science*, **22**, 193-196.

[11] Liu, J.K. (1999) Unraveling the Enigma of the Disappearance of Water Bloom from the East Lake (Lake Donghu) of Wuhan. *Resour Environ Yangtze Basin*, **8**, 312-319.

[12] Ke, Z., Xie, P. and Guo, L. (2008) In Situ Study on Effect of Food Competition on Diet Shifts and Growth of Silver and Bighead Carps in Large Biomanipulation Fish Pens in Meiliang Bay, Lake Taihu. *Journal of Applied Ichthyology*, **24**, 263-268. https://doi.org/10.1111/j.1439-0426.2008.01060.x

[13] Guo, L.G., Wang, Q., Xie, P., *et al.* (2015) A Non-Classical Biomanipulation Experiment in Gonghu Bay of Lake Taihu: Control of Microcystis Blooms Using Silver and Bighead Carp. *Aquaculture Research*, **46**, 2211-2224. https://doi.org/10.1111/are.12375

[14] Zhang, X., Xie, P., Hao, L., *et al.* (2006) Effects of the Phytoplanktivorous Silver Carp (Hypophthalmichthys molitrixon) on Plankton and the Hepatotoxic Microcystins in an Enclosure Experiment in a Eutrophic Lake, Lake Shichahai in Beijing. *Aquaculture*, **257**, 173-186. https://doi.org/10.1016/j.aquaculture.2006.03.018

[15] Starling, F. (1993) Control of Eutrophication by Silver Carp (Hypophthalmichthys molitrix) in the Tropical ParanoA Reservoir (Brasilia, Brazil): A Mesocosm Experiment. *Hydrobiologia*, **257**, 43-152. https://doi.org/10.1007/BF00765007

[16] Li, D.S. and Dong, S.L. (1996) The Structure and Function of the Filtering Apparatus of Silver Carp and Bighead Carp. *Acta Zoologica Sinica*, **42**, 10-14.

[17] Volterra, V. (1926) Fluctuations in the Abundance of a Species Considered Mathematically. *Nature*, **118**, 558-560. https://doi.org/10.1038/118558a0

[18] Lotka, A.J. (1925) Elements of Physical Biology. Williams and Wilkins, Baltimore.

[19] Baurmanna, M., Gross, T. and Feudel, U. (2007) Instabilities in Spatially Extended Predator-Prey Systems: Spatio-Temporal Patterns in the Neighborhood of Turing-Hopf bifurcations. *Journal of Theoretical Biology*, **245**, 220-229. https://doi.org/10.1016/j.jtbi.2006.09.036

[20] Freedman, H. (1980) Deterministic Mathematical Models in Population Ecology. Marcel Dekker, New York.

[21] Turchin, P. (2013) Complex Population Dynamics. Princeton University Press, Princeton.

[22] Xiao, M. and Cao, J. D. (2009) Hopf Bifurcation and Non-Hyperbolic Equilibrium in a Ratiodependent Predator-Prey Model with Linear Harvesting Rate: Analysis and Computation. *Mathematical and Computer Modelling*, **50**, 360-379. https://doi.org/10.1016/j.mcm.2009.04.018

[23] Zhang, L., Wang, W.J. and Xue, Y.K. (2009) Spatiotemporal Complexity of a Predator-Prey System with Constant Harvest Rate. *Chaos Solitons & Fractals*, **41**, 38-46. https://doi.org/10.1016/j.chaos.2007.11.009

[24] Chang, X.Y. and Wei, J.J. (2012) Hopf Bifurcation and Optimal Control in a Diffusive Predator-Prey System with Time Delay and Prey Harvesting. *Nonlinear Analysis-Modelling and Control*, **17**, 379-409.

[25] Kar, T. (2006) Modelling and Analysis of a Harvested Prey-Predator System Incorporating a Prey Refuge. *Journal of Computational and Applied Mathematics*, **185**, 19-33. https://doi.org/10.1016/j.cam.2005.01.035

[26] Lenzini, P. and Rebaza, J. (2010) Non-Constant Predator Harvesting on Ratio-Dependent Predator-Prey Models. *Advances and Applications in Mathematical Sciences*, **4**, 791-803.

[27] Feng, P. (2014) On a Diffusive Predator-Prey Model with Nonlinear Harvesting. *Mathematical Biosciences and Engineering*, **11**, 807-821. https://doi.org/10.3934/mbe.2014.11.807

[28] Li, Y. and Wang, M. (2015) Dynamics of a Diffusive Predator-Prey Model with Modified Leslie-Gower Term and Michaelis-Menten Type Prey Harvesting. *Acta Applicandae Mathematicae*, **140**, 398-410. https://doi.org/10.1007/s10440-014-9983-z

[29] Chakraborty, S., Pal, S. and Bairagi, N. (2012) Predator-Prey Interaction with Harvesting: Mathematical Study with Biological Ramifcations. *Applied Mathematical Modelling*, **36**, 4044-4059. https://doi.org/10.1016/j.apm.2011.11.029

[30] Clark, C.W. (2010) Mathematical Bioeconomics: The Mathematics of Conservation. John Wiley and Sons, New Jersey.

[31] Martin, A. and Ruan, S. (2001) Predator-Prey Models with Delay and Prey Harvesting. *Journal of Mathematical Biology*, **43**, 247-267. https://doi.org/10.1007/s002850100095

[32] Courchamp, F., Clutton-Brock, T. and Grenfell, B. (1999) Inverse Density Dependence and the Allee Effect. *Trends in Ecology & Evolution*, **14**, 405-410. https://doi.org/10.1016/S0169-5347(99)01683-3

[33] Stephens, P.A., Sutherland, W.J. and Freckleton, R.P. (1999) What Is the Allee Effect. *Oikos*, **87**, 185-190. https://doi.org/10.2307/3547011

[34] Stephens, P.A. and Sutherland, W.J. (1999) Consequences of the Allee Effect for Behaviour, Ecology and Conservation. *Trends in Ecology & Evolution*, **14**, 401-405. https://doi.org/10.1016/S0169-5347(99)01684-5

[35] Deredec, A. and Courchamp, F. (2003) Extinction Thresholds in Host-Parasite Dynamics. *Annales Zoologici Fennici*, **40**, 115-130.

[36] Wang, M.H. and Kot, M. (2001) Speeds of Invasion in a Model with Strong or Weak Allee effects. *Mathematical Biosciences*, **171**, 83-97. https://doi.org/10.1016/S0025-5564(01)00048-7

[37] Aguirre, P., González-Olivares, E. and Sáez, E. (2009) Two Limit Cycles in a Leslie-Gower Predator-Prey Model with Additive Allee Effect. *Nonlinear Analysis: Real World Applications*, **10**, 1401-1416. https://doi.org/10.1016/j.nonrwa.2008.01.022

[38] Aguirre, P., González-Olivares, E. and Sáez, E. (2009) Three Limit Cycles in a Leslie-Gower Predator-Prey Model with Additive Allee effect. *SIAM Journal on Applied Mathematics*, **69**, 1244-1262. https://doi.org/10.1137/070705210

[39] Sen, M., Banerjee, M. and Morozov, A. (2012) Bifurcation Analysis of a Ratio-Dependent Prey-Predator Model with the Allee Effect. *Ecological Complexity*, **11**, 12-27. https://doi.org/10.1016/j.ecocom.2012.01.002

[40] Wang, J., Shi, J. and Wei, J. (2011) Predator-Prey System with Strong Allee Effect in prey. *Journal of Mathematical Biology*, **62**, 291-331. https://doi.org/10.1007/s00285-010-0332-1

[41] Sen, M., Banerjee, M. and Takeuchi, Y. (2018) Influence of Allee effect in Prey Populations on the Dynamics of Two-Prey-One-Predator Model. *Mathematical Biosciences and Engineering*, **15**, 883-904. https://doi.org/10.3934/mbe.2018040

[42] Liu, H., Li, Z., Gao, M., Dai, H. and Liu, Z. (2009) Dynamics of a Host-Parasitoid model with Allee Effect for the Host and Parasitoid Aggregation. *Ecological Complexity*, **6**, 337-345. https://doi.org/10.1016/j.ecocom.2009.01.003

[43] Liu, H., Ye, Y., Wei, Y., Ma, M. and Zhang, K. (2019) Pattern Formation in a Reaction-Diffusion Predator-Prey Model with Weak Allee Effect and Delay. *Complexity*, **2019**, Article ID: 6282958. https://doi.org/10.1155/2019/6282958

[44] Wang, W., Zhu, Y.N. and Cai, Y. Wang, W. (2014) Dynamical Complexity Induced by Allee Effect in a Predator-Prey Model. *Nonlinear Analysis: Real World Applications*. **16**, 103-119. https://doi.org/10.1016/j.nonrwa.2013.09.010

[45] Perko, L. (2001) Differential Equations and Dynamical Systems Differential Equations and Dynamical Systems. In: Bloch A., Epstein, C.L., Goriely, A. and Greengard, L., Eds., *Texts in Applied Mathematics*, Springer, Berlin, I-XIV. https://doi.org/10.1007/978-1-4613-0003-8

[46] Zhang, Z.F., Huang, W.Z. and Dong, Z.X. (1992) Qualitative Theory of Differential Equation. Science Press, Beijing.

[47] Cooke, K.L. and Grossman, Z. (1982) Discrete Delay, Distributed Delay and Stability Switches. *Journal of Mathematical Analysis Applications*, **86**, 592-627.

https://doi.org/10.1016/0022-247X(82)90243-8

[48] Hu, D.P. and Cao, H.J. (2017) Stability and Bifurcation Analysis in a Predator-Prey System with Michaelis-Menten Type Predator Harvesting. *Nonlinear Analysis: Real World Applications*, **33**, 58-82. https://doi.org/10.1016/j.nonrwa.2016.05.010